US 20090114273A1

(19) **United States**

(12) **Patent Application Publication**

Kamat

(10) **Pub. No.: US 2009/0114273 A1**

(43) **Pub. Date: May 7, 2009**

(54) **NANOMATERIAL SCAFFOLDS FOR ELECTRON TRANSPORT**

(75) Inventor: **Prashant Kamat**, Granger, IN (US)

Correspondence Address:
SCHWABE, WILLIAMSON & WYATT, P.C.
PACWEST CENTER, SUITE 1900
1211 SW FIFTH AVENUE
PORTLAND, OR 97204 (US)

(73) Assignee: **University of Notre Dame du Lac**, Notre Dame, IN (US)

(21) Appl. No.: **12/136,879**

(22) Filed: **Jun. 11, 2008**

Related U.S. Application Data

(60) Provisional application No. 60/934,403, filed on Jun. 13, 2007.

Publication Classification

(51) **Int. Cl.**
H01L 31/00 (2006.01)
H01B 1/04 (2006.01)

(52) **U.S. Cl.** **136/252**; 252/501.1; 977/748; 977/831

(57) **ABSTRACT**

Embodiments of the present invention provide nanomaterial scaffolds for transporting electrons. There is provided a single wall carbon nanotube (SWCNT) architecture employed as a conducting scaffold in semiconductor based photoelectrochemical cells. SWCNT architecture provides a nanotube network to disperse nanoparticles and/or quantum dots, whether ordered or randomized. As a result, an increase in incident photon conversion to charge carrier conversion efficiency (IPCE) represents a beneficial role of SWCNT architecture as a conducting scaffold to facilitate charge collection and charge transport in nanostructured semiconductor films. Embodiments may be used for solar cells based on semiconductor quantum dots and nanostructures, solar hydrogen production, microcapacitors and storage batteries, solar-fuel cell hybrids, etc.

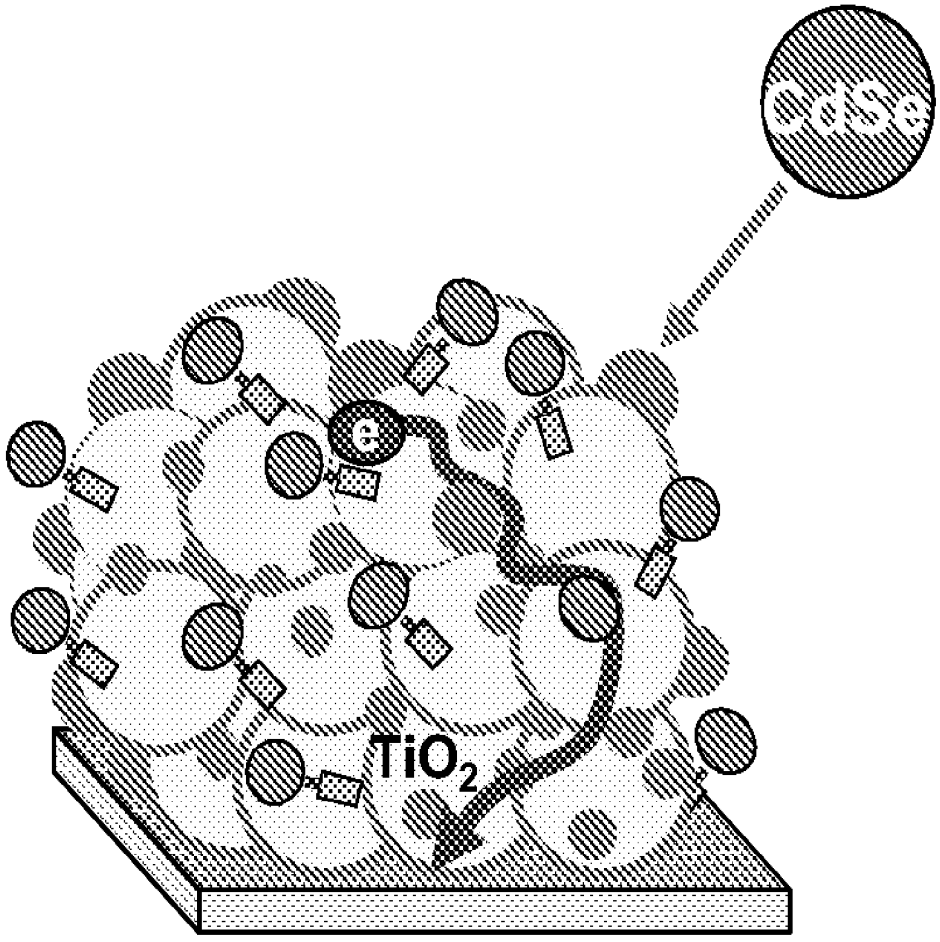

OTE/TiO_2 nanoparticles

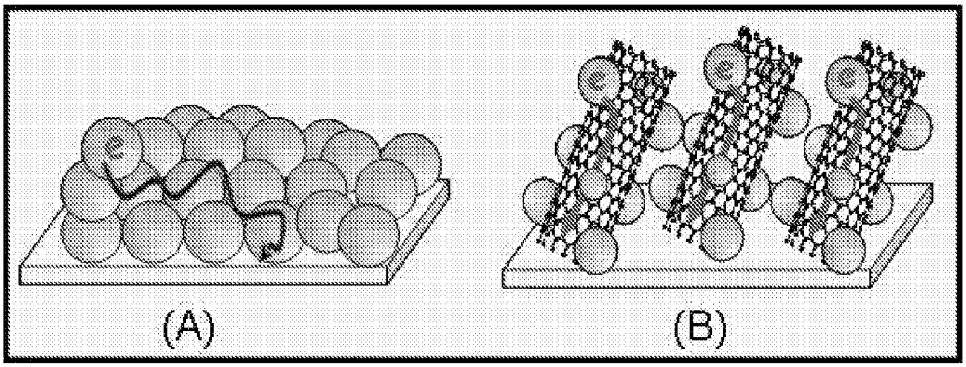

FIGURE 1A
Prior Art

FIGURE 1B

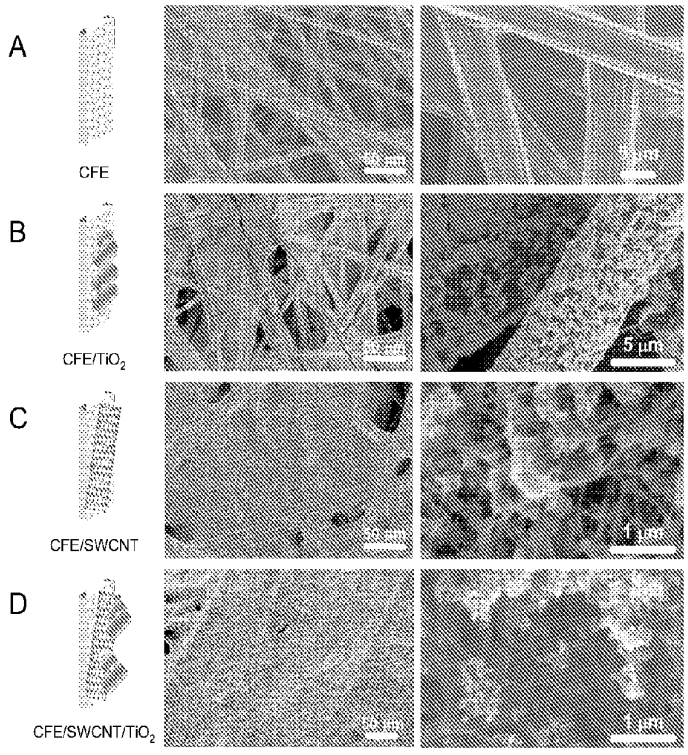

FIGURE 2

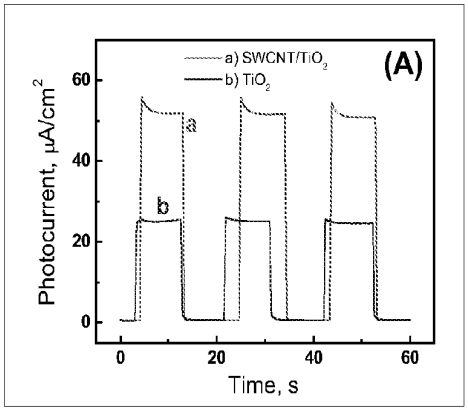

FIGURE 3A

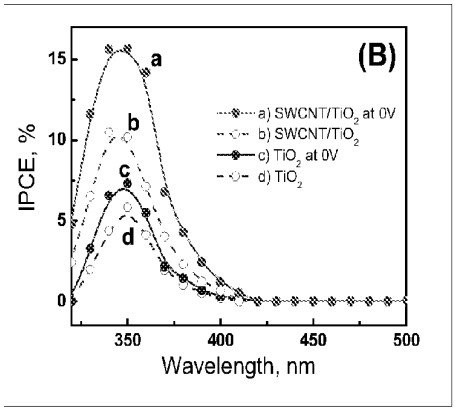

FIGURE 3B

FIGURE 4

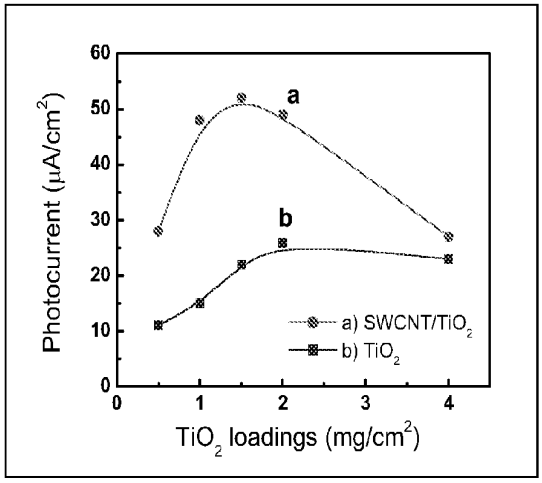

FIGURE 5

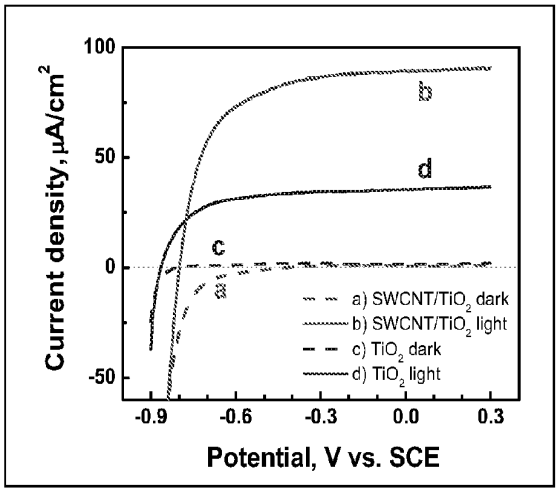

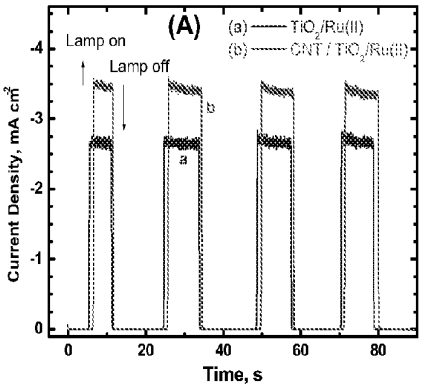

FIGURE 6A

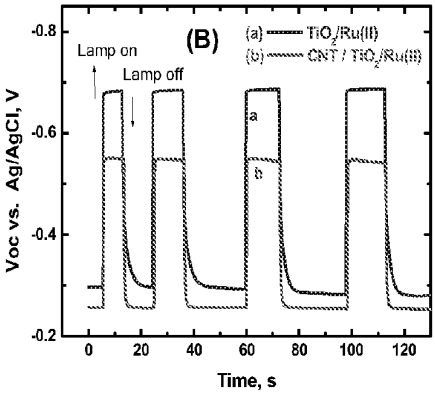

FIGURE 6B

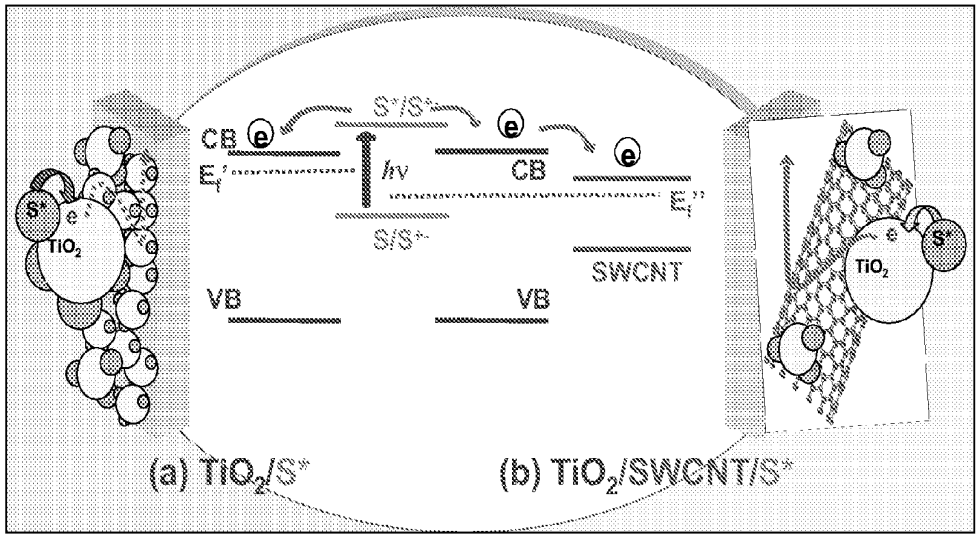

FIGURE 7

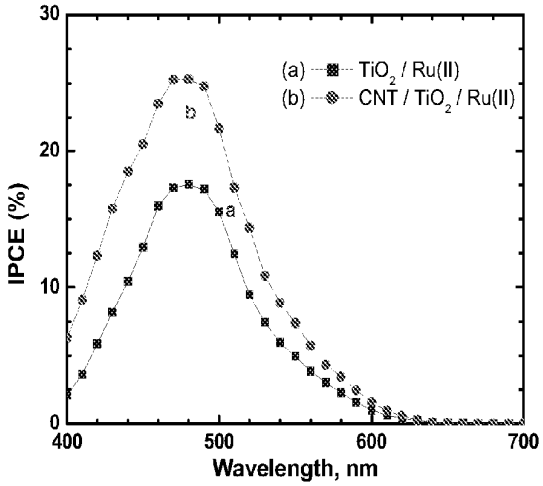

FIGURE 8

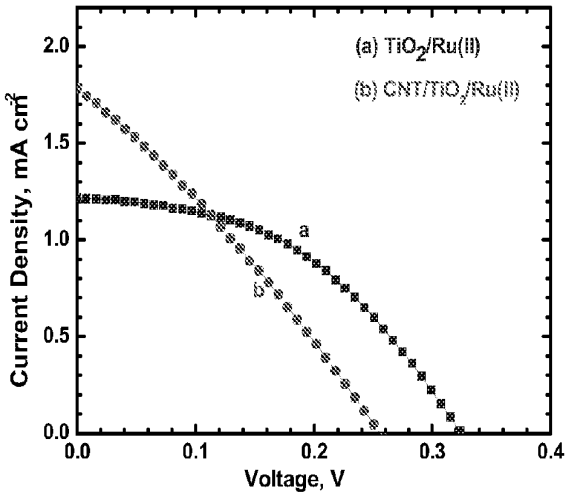

FIGURE 9

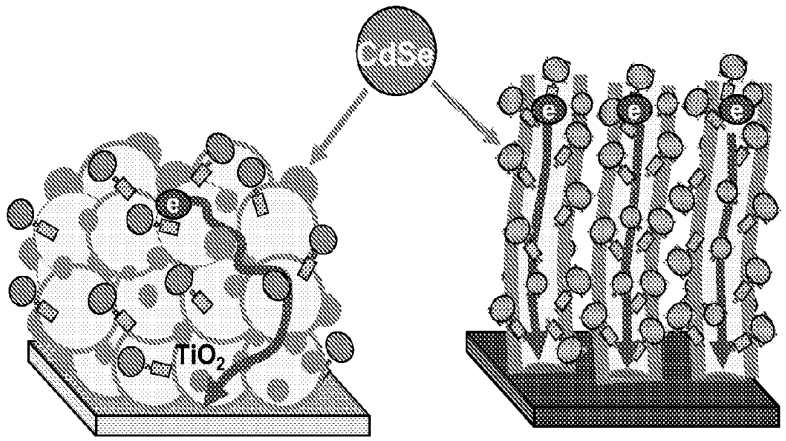

OTE/TiO_2 nanoparticles

FIGURE 10A

Ti/TiO_2 nanotubes

FIGURE 10B

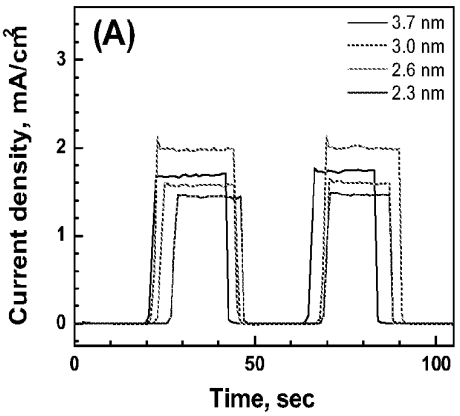

FIGURE 11A

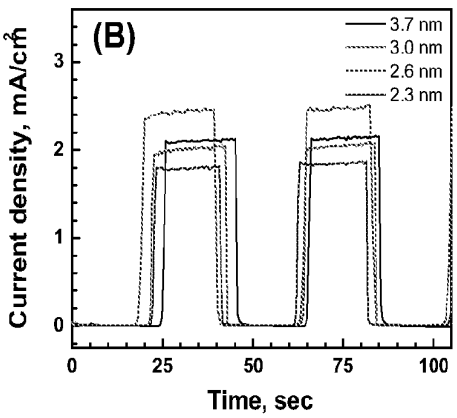

FIGURE 11B

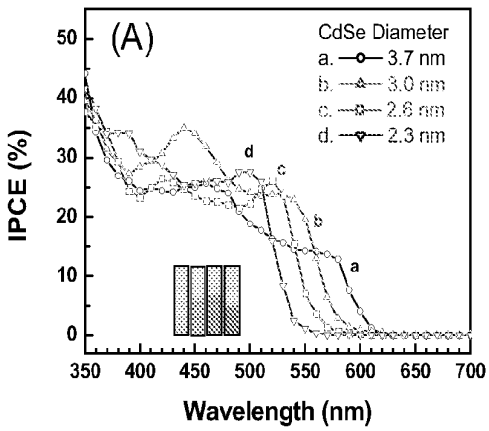

FIGURE 12A

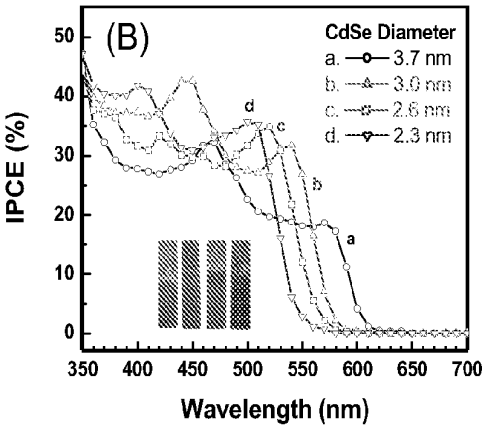

FIGURE 12B

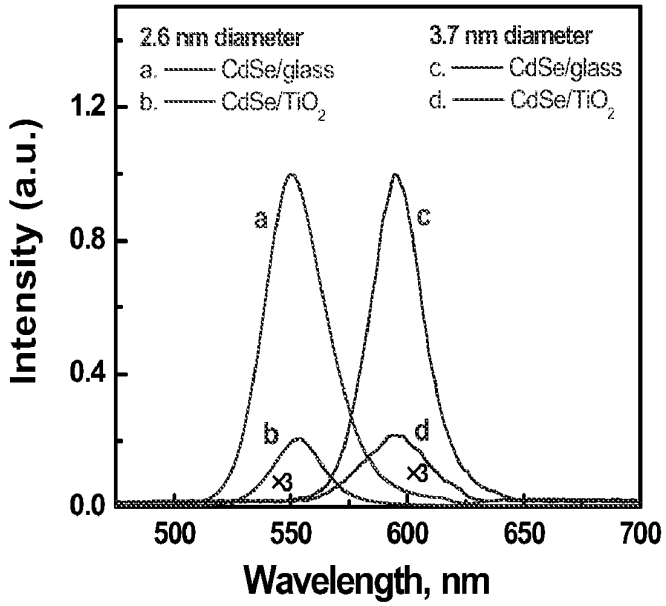

FIGURE 13

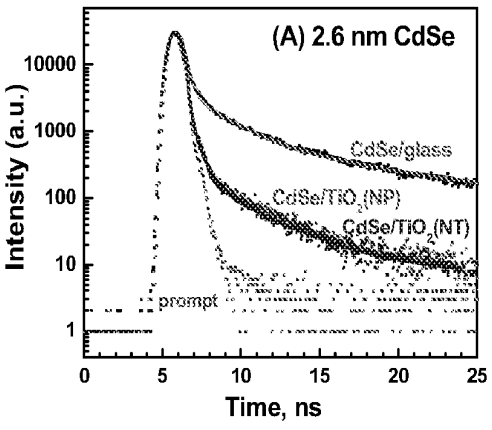

FIGURE 14A

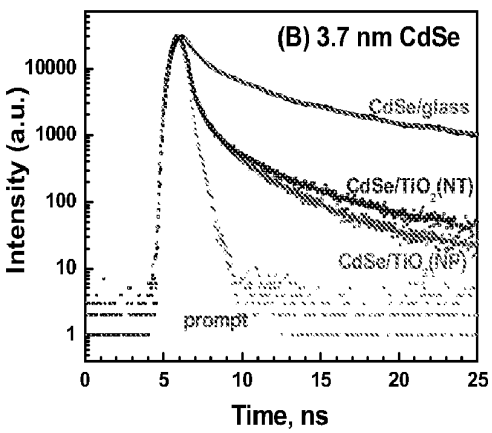

FIGURE 14B

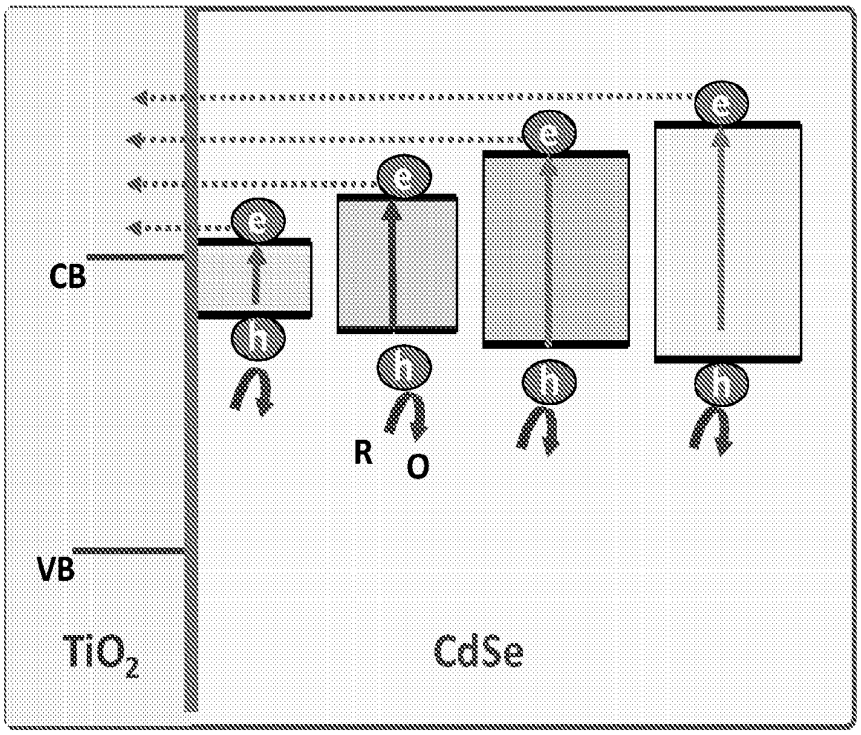

FIGURE 15

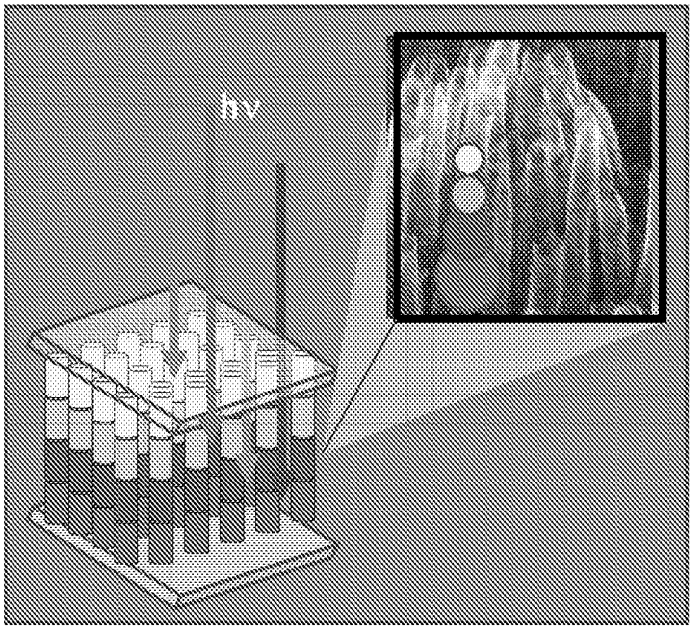

FIGURE 16

NANOMATERIAL SCAFFOLDS FOR ELECTRON TRANSPORT

CROSS REFERENCE TO RELATED APPLICATIONS

[0001] The present application claims priority to U.S. Provisional Patent Application No. 60/934,403, filed Jun. 13, 2007, entitled "Single Wall Carbon Nanotube Scaffolds for Boosting the Efficiency of Solar Cells," the entire disclosure of which is hereby incorporated by reference in its entirety.

GOVERNMENT INTERESTS

[0002] This invention was made with Government support under Grant/Contract No. DE-FC02-04ER15533 awarded by the US Department of Energy. The Government may have certain rights in the invention.

TECHNICAL FIELD

[0003] Embodiments of the present invention relate to the fields of nanotechnology and energy, and, more specifically, to nanomaterial scaffolds for transporting electrons, such as for use in photoelectrochemical solar cells.

BACKGROUND

[0004] The photocatalytic activity of semiconductor films has been widely explored in designing solar cells, solar hydrogen production and environmental remediation. Of particular interest is the dye-sensitized solar cell (DSSC) which uses mesoscopic TiO_2 films modified with sensitizing dyes. Despite the initial success of achieving 10% solar conversion efficiency, the effort to further improve their performance has not resulted in breakthroughs. A major hurdle in attaining higher photoconversion efficiency in such nanostructured electrodes is the transport of electrons across the particle network. The photogenerated electrons in mesoscopic films for example have to travel through the network of semiconductor particles and encounter many grain boundaries during the transit. Such a random transit path for the photogenerated electrons increases the probability of their recombination with oxidized sensitizer. The use of a redox couple such as I_3^-/I^- facilitates the electron transport to some extent by rapid regeneration of the oxidized sensitizer. However, the conversion efficiency is still not entirely favorable.

BRIEF DESCRIPTION OF THE DRAWINGS

[0005] Embodiments of the present invention will be readily understood by the following detailed description in conjunction with the accompanying drawings. Embodiments of the invention are illustrated by way of example and not by way of limitation in the figures of the accompanying drawings.

[0006] FIGS. **1**A and **1**B illustrate electron transport across a semiconductor particle based film (FIG. **1**A; prior art), and in the presence of a nanotube support architecture (FIG. **1**B) in accordance with various embodiments of the present invention;

[0007] FIG. **2**, rows A-D, illustrate scanning electron micrographs of carbon fiber electrodes (CFE) at different stages of modification: (A) before surface modification, (B) after modification with TiO_2 particles, (C) after electrophoretic deposition of SWCNT, and (D) after deposition of TiO_2 particles onto SWCNT film;

[0008] FIG. **3**A illustrates photocurrent response versus time profiles of CFE/SWCNT/TiO_2 (a) and CFE/TiO_2 (b) electrodes at 0 V versus SCE; light intensity was 50 mW/cm^2 (λ>300 nm). FIG. **3**B illustrates photocurrent action spectra of CFE/SWCNT/TiO_2 (a, b) and CFE/TiO_2 (c, d) electrodes at no applied bias (b, d) and at 0 V versus SCE (a, c); IPCE(%) $=(1240\times i_{sc})(\lambda\times I_{inc})\times 100$ where i_{sc} is short circuit current and I_{inc} is the power of the incident light; electrolyte was N_2-sat 1 M KOH solution;

[0009] FIG. **4** illustrates photocurrent response as a function of the amount of TiO_2 deposited on CFE or CFE/SWCNT electrodes; SWCNT concentration was maintained constant at 0.2 mg/cm^2 while TiO_2 loading was varied;

[0010] FIG. **5** illustrates I-V characteristics for OTE/TiO_2 (c, d) and OTE/SWCNT/TiO_2 (a, b) obtained with (b, d) and without (a, c) light illumination from the backside of the OTE; TiO_2 and SWCNT loadings were 2 and 0.01 mg/cm^2 respectively;

[0011] FIGS. **6**A and **6**B illustrate photocurrent and photovoltage response, respectively, of (a) OTE/TiO_2/Ru(II) and (b) OTE/SWCNT/TiO_2/Ru(II) electrodes; light intensity was 50 mW/cm^2 (λ>400 nm); electrolyte was 0.5 M LiI and 0.05 M I_2 in acetonitrile;

[0012] FIG. **7** is an energy diagram illustrating the charge injection from excited sensitizer (S*) into TiO_2 and transport of photoinjected electrons to the electrode surface without (a) and with (b) SWCNT network; the Fermi level of TiO_2 (E_f') shifts to more positive potentials (E_f') as it equilibrates with SWCNT;

[0013] FIG. **8** illustrates photocurrent action spectra of (a) OTE/TiO_2/Ru(II), and (b) OTE/SWCNT/TiO_2/Ru(II) electrodes; IPCE(%)$=(1240\times i_{sc})/(\lambda\times I_{inc})\times 100$ where i_{sc} is short circuit current and I_{inc} is the power of the incident light; electrolyte was 0.5 M LiI and 0.05 M I_2 in acetonitrile;

[0014] FIG. **9** illustrates power characteristics of a photoelectrochemical cell employing (a) OTE/TiO_2/Ru(II), and (b) OTE/SWCNT/TiO_2/Ru(II) electrodes; electrolyte was 0.5 M LiI and 0.05 M I_2 in acetonitrile;

[0015] FIGS. **10**A and **10**B illustrate random versus directed electron transport through support architectures; FIG. **10**A illustrates TiO_2 particle architecture, and FIG. **10**B illustrates TiO_2 nanotube films modified with CdSe quantum dots;

[0016] FIG. **11**A illustrates photocurrent response of OTE/TiO_2(NP)/CdSe and FIG. **11**B illustrates photocurrent response of Ti/TiO_2(NT)/CdSe electrodes; individual traces correspond to (a) 2.3, (b) 2.6, (c) 3.0, and (d) 3.7 nm diameter CdSe quantum dots anchored on nanostructured TiO_2 films (excitation >420 nm, 100 mW/cm^2, electrolyte: 0.1 M Na_2S solution);

[0017] FIGS. **12**A and **12**B illustrate photocurrent action spectra recorded in terms of incident photon to charge carrier generation efficiency (IPCE) of OTE/TiO_2(NP)/CdSe and Ti/TiO_2(NT)/CdSe electrodes, respectively; the individual IPCE responses correspond to (a) 2.3, (b) 2.6, (c) 3.0, and (d) 3.7 nm diameter CdSe quantum dots anchored on nanostructured TiO_2 films;

[0018] FIG. **13** illustrates emission spectra of (a, b) 2.6 nm and (c, d) 3.7 nm diameter CdSe quantum dot films deposited on glass (a, c) and TiO_2 films, (b, d) excitation was at 480 nm; the spectra (b) and (d) carry a multiplication factor of 3; all spectra were recorded using front face geometry;

[0019] FIGS. **14**A and **14**B illustrate emission decay of 2.6 nm (emission at 540 nm) and 3.7 nm diameter (emission at

580 nm) CdSe quantum dots deposited on a glass slide, TiO_2 nanoparticulate film, and TiO_2 nanotube array; excitation wavelength was 457 nm; solid lines represent kinetic fit using triexponential decay analysis; prompt measurement of instrument response used to mathematically deconvolute best-fit curve is also shown;

[0020] FIG. **15** is a schematic diagram illustrating the energy levels of different size CdSe quantum dots and TiO_2; the injection of electrons from CdSe quantum dots into TiO_2 is influenced by the energy difference between the two conduction bands (band positions are for reference only and not drawn to scale); and

[0021] FIG. **16** is a schematic illustration of a rainbow solar cell assembled with different size CdSe quantum dots on a TiO_2 nanotube array.

DETAILED DESCRIPTION OF EMBODIMENTS OF THE INVENTION

[0022] In the following detailed description, reference is made to the accompanying drawings which form a part hereof, and in which are shown by way of illustration embodiments in which the invention may be practiced. It is to be understood that other embodiments may be utilized and structural or logical changes may be made without departing from the scope of the present invention. Therefore, the following detailed description is not to be taken in a limiting sense, and the scope of embodiments in accordance with the present invention is defined by the appended claims and their equivalents.

[0023] Various operations may be described as multiple discrete operations in turn, in a manner that may be helpful in understanding embodiments of the present invention; however, the order of description should not be construed to imply that these operations are order dependent.

[0024] The description may use perspective-based descriptions such as up/down, back/front, and top/bottom. Such descriptions are merely used to facilitate the discussion and are not intended to restrict the application of embodiments of the present invention.

[0025] The terms "coupled" and "connected," along with their derivatives, may be used. It should be understood that these terms are not intended as synonyms for each other. Rather, in particular embodiments, "connected" may be used to indicate that two or more elements are in direct physical or electrical contact with each other. "Coupled" may mean that two or more elements are in direct physical or electrical contact. However, "coupled" may also mean that two or more elements are not in direct contact with each other, but yet still cooperate or interact with each other.

[0026] For the purposes of the description, a phrase in the form "A/B" or in the form "A and/or B" means (A), (B), or (A and B). For the purposes of the description, a phrase in the form "at least one of A, B, and C" means (A), (B), (C), (A and B), (A and C), (B and C), or (A, B and C). For the purposes of the description, a phrase in the form "(A)B" means (B) or (AB) that is, A is an optional element.

[0027] The description may use the phrases "in an embodiment," or "in embodiments," which may each refer to one or more of the same or different embodiments. Furthermore, the terms "comprising," "including," "having," and the like, as used with respect to embodiments of the present invention, are synonymous.

[0028] Embodiments of the present invention provide nanomaterial scaffolds for transporting electrons.

[0029] In an embodiment, there is provided a single wall carbon nanotube (SWCNT) architecture employed as a conducting scaffold in semiconductor based photoelectrochemical cells. In an embodiment, such a configuration may boost photoconversion efficiency. In an embodiment, such a configuration may boost photoconversion efficiency by a factor of two or more.

[0030] In an embodiment, SWCNT architecture provides a nanotube network to disperse titanium dioxide (TiO_2) particles, or other nanoparticles, such as SnO_2 or others. In an embodiment, an increase in incident photon conversion to charge carrier conversion efficiency (IPCE) represents a beneficial role of SWCNT architecture as a conducting scaffold to facilitate charge collection and charge transport in nanostructured semiconductor films. Such nanotube/nanoparticle architecture may provide a variety of benefits, including improving the efficiency of nanostructure based solar cells, e.g., dye sensitized solar cells, or in water photoelectrolysis. Embodiments may be used for solar cells based on semiconductor quantum dots and nanostructures, solar hydrogen production, microcapacitors and storage batteries, solar-fuel cell hybrids, etc.

[0031] In an embodiment, there is provided a nanostructured material, comprising a single wall carbon nanotube having a first and second end and an outer and inner surface, the first end of the single wall carbon nanotube coupled to a substrate, and a plurality of nanoparticles coupled to the single wall carbon nanotube.

[0032] In an embodiment, TiO_2 nanoparticles may be dispersed on single wall carbon nanotubes to improve photoinduced charge separation and transport of carriers to the collecting electrode surface. In accordance with an embodiment, a shift of ~100 mV in apparent Fermi level of an SWCNT/TiO_2 system as compared to an unsupported TiO_2 system indicates the Fermi level equilibration between the two systems.

[0033] In an embodiment of the invention, one dimensional nanostructures may be used to direct the flow of photogenerated charge carriers. In an embodiment, a nanotube network may be used as a support to anchor light harvesting semiconductor particles and may facilitate the electron transport to the collecting electrode surface/substrate in a photovoltaic/solar cell. Scenarios that illustrate the electron transport in a semiconductor particle based film and an exemplary nanotube-nanoparticle composite are presented in FIGS. **1**A and **1**B, respectively. The particle based film and nanotube-nanoparticle composite are shown coupled to a collecting electrode surface/substrate, which may be, in an embodiment, part of a photovoltaic/solar cell. In a further embodiment, the collecting electrode surface/substrate may be further coupled to one or more other electronic components for further handling/processing of the harvested energy.

[0034] In embodiments, the term "substrate" may refer to any suitable substrate used, for example, as a collecting electrode surface/substrate, including one or more of silicon, metal, polymers, etc.

[0035] The unique electrical and electronic properties, wide electrochemical stability window, and high surface area render SWCNT beneficial as a scaffold to anchor light harvesting assemblies. In accordance with an embodiment, the electron accepting ability of semiconducting SWCNT thus offers an opportunity to facilitate electron transport and thus increase the photoconversion efficiency of nanostructure semiconductor based solar cells. In further embodiments,

semiconductor particles, such as CdSe and CdTe, may be attached to carbon nanotubes directly, to other nanoparticles, and/or via functional linker molecules and may induce charge transfer processes under visible light irradiation.

[0036] SWCNT networks may be constructed using a variety of methods. In accordance with an exemplary embodiment, FIG. **2** shows low and high magnification scanning electron micrographs (SEM images) of carbon fiber paper (carbon fiber electrodes (CFE)) at different stages of modification. Preparation of the carbon fiber paper may be done using any of a variety of methods, including as described in Kongkanand et al., Single Wall Carbon Nanotube Scaffolds for Photoelectrochemical Solar Cells Capture and Transport of Photogenerated Electrons, Nano Lett., Vol. 7, No. 3, 676-680 (2007), the entire contents of which are hereby incorporated by reference. These images provide a perspective of the overall electrode morphology and the ability to anchor TiO_2 nanoparticles on CFE and SWCNT networks with a good dispersibility. The carbon fibers of the CFE electrode are in micron size (row A) and they serve as the backbone of the electrode in collecting photogenerated electrons and communicating with the external circuit. When TiO_2 particles are dispersed on the CFE, they get dispersed quite uniformly on the carbon microfibers (row B). The higher magnification micrograph confirms the ability of carbon microfibers to support TiO_2 photocatalyst particles and collect photogenerated electrons.

[0037] In accordance with another embodiment, SWCNT was deposited on the carbon fiber electrode using an electrophoretic deposition method. This allowed extension of the carbon support network at a nanometer scale. At low magnifications the SWCNT film may be seen covering the voids in the larger carbon microfiber network (row C). The magnified view of the same film shows a close interwoven network of SWCNT bundles. In an embodiment, the CFE/SWCNT was further modified by casting a film of TiO_2 nanoparticles. The figures in row D show the micrograph of the electrode obtained after deposition of TiO_2 nanoparticles on the SWCNT network. In the selected high magnification image, both TiO_2 particle aggregates and the underlying SWCNT network are shown. However, most of the other areas show complete coverage of TiO_2 particles. In an embodiment, the aggregation of TiO_2 particles becomes predominant when the ratio of TiO_2 to SWCNT is increased. If the TiO_2 coverage is kept sufficiently low, in an embodiment, the SWCNT network is expected to interact quite effectively with TiO_2 particles and facilitate charge transport in the composite film.

[0038] Films of TiO_2 particles undergo charge separation upon excitation with UV-light (E_g>3.2 eV). When employed as photoanodes in a photoelectrochemical cell, TiO_2 particulate films cast on electrode surfaces exhibit anodic photocurrent generation. The magnitude of the photocurrent represents the charge collection efficiency of the electrode surface. FIG. **3**A shows the short circuit photocurrent generation at CFE/TiO_2 and CFE/SWCNT/TiO_2 electrodes. Both electrodes are prompt in generating photocurrent with a reproducible response to ON-OFF cycles. In an embodiment, the TiO_2 particles deposited on the SWCNT network exhibit an enhanced photocurrent.

[0039] In an embodiment, when in contact with photoirradiated TiO_2 nanoparticles, SWCNTs may accept and store electrons. The Fermi level equilibration with photoirradiated TiO_2 particles indicates storage of up to 1 electron per 32 carbon atoms in the SWCNT. The stored electrons are readily discharged on demand upon addition of electron acceptors such as thiazine and oxazine dyes (i.e., acceptors having a lower reduction potential than the SWCNT conduction band) to the SWCNT/TiO_2 suspension. The ability of SWCNT to accept electrons and transfer them to a suitable electron acceptor highlights the mediating role that these nanotubes may play in a charge transfer process.

[0040] The stepwise electron transfer from photoirradiated TiO_2 nanoparticles to SWCNT to redox couple has enabled the probing of the electron equilibration process and determination of the apparent Fermi level of the SWCNT/TiO_2 system. SWCNTs undergo charge equilibration with semiconductor particles such as TiO_2 and attain an apparent Fermi level lower (20-30 mV in suspensions and 130 mV in films) than the Fermi level of semiconductor TiO_2. A positive shift in apparent Fermi level indicates the ability of SWCNTs to undergo charge equilibration with photoirradiated TiO_2 particles.

[0041] In an embodiment, the effect of electron equilibration between TiO_2 and SWCNT on the photoelectrochemical effect in TiO_2 and SWCNT/TiO_2 films was explored. The films of TiO_2 and SWCNT/TiO_2 were cast on conducting glass electrodes as described previously. These films are photoactive and generate photocurrent under UV-excitation when employed as a photoanode in a photoelectrochemical cell. The primary process responsible for photocurrent generation is the charge separation in TiO_2 particles as they are subjected to bandgap (E_g>3.2 eV) excitation.

[0042] Under open circuit conditions, the electrons accumulate and equilibrate with the redox couple in the electrolyte. The measured open circuit voltage is the difference between the apparent Fermi level of the semiconductor film and the reduction potential of the redox couple employed. Thus, open-circuit voltage is a direct measure of the apparent Fermi-level of the semiconductor film if one employs the same redox couple. The photovoltage response of optically transparent electrode OTE/TiO_2 and OTE/SWCNT/TiO_2 electrodes shows a rise in photovoltage in two steps: a prompt increase followed by a slow growth as the electrode system equilibrated with the redox couple. Notably, the magnitude of the photovoltage was 130 mV lower for OTE/SWCNT/TiO_2 electrode. The lower photovoltage further supports the notion that the SWCNT/TiO_2 composite has a lower apparent Fermi level than the pristine TiO_2 system. Similar to the charge equilibration effects in suspension, the electrons are transferred from TiO_2 to SWCNT and thus attain a lower equilibrium potential.

[0043] It is interesting to note that the photovoltage decay of OTE/SWCNT/TiO_2 is slower than that of OTE/TiO_2 electrode. This observation further indicates the involvement of SWCNT in participating in the electron storage and equilibration process, and thus increasing the survivability of accumulated electrons. Indeed, the ability of SWCNT to accept and transport electrons in the SWCNT/TiO_2 films has a beneficial effect in overall photocurrent generation. In an embodiment, an approximately two-fold increase of incident photon-to-photocurrent generation efficiency was achieved by employing a SWCNT conducting scaffold in TiO_2-nanostructure based photoelectrochemical cells.

[0044] In an embodiment, electrode performance was further evaluated by recording the IPCE by monitoring the photocurrent at different incident wavelengths. The photocurrent action spectra of the two electrodes at short circuit and 0 V vs. SCE (standard calomel electrode) are shown in FIG. **3**B. Both

of these electrodes have a photocurrent onset at 380 nm corresponding to the bandgap of TiO_2. In the absence of SWCNT network, a maximum IPCE of 7.36% (350 nm) at 0 V vs. SCE was observed. The IPCE response shows a significant enhancement with an IPCE of 16% when a SWCNT scaffold supports the TiO_2 particles. Nearly doubling of the photoconversion efficiency is an indication of the improved charge collection efficiency using a SWCNT network.

[0045] In accordance with an embodiment, fuel cell experiments carried out with a Pt/SWCNT system shows that both semiconducting and metallic carbon nanotubes contribute to improving the charge transfer and charge collection in both cathodic and anodic compartments. In an embodiment, such charge transport properties of carbon nanotubes may also improve photocurrent generation.

[0046] In an embodiment, the role of SWCNT in enhancing the photoelectrochemical performance of TiO_2 film was probed by varying the ratio of SWCNT/TiO_2 in the composite film. The concentration of the SWCNT was kept constant while TiO_2 loading was varied. FIG. **4** compares the photocurrent observed with CFE/TiO_2 and CFE/SWCNT/TiO_2 electrodes at different loading of TiO_2 particles. In the case of the CFE/TiO_2 film, an increase in photocurrent is observed with increased TiO_2 loading (at loadings below 2 mg/cm^2) as more excited TiO_2 particles undergo charge separation and participate in the photocurrent generation. At higher TiO_2 loadings, saturation in the photocurrent is observed showing the limitations of light absorption within the TiO_2 film. In the case of CFE/SWCNT/TiO_2, a similar increasing trend is observed at TiO_2 loadings up to 1.5 mg/cm^2. The photocurrent observed at these TiO_2 loadings is significantly greater than the photocurrent observed without the SWCNT support. This increase in the photoconversion efficiency shows that the SWCNT support architecture plays an important role in improving the charge transport properties within the composite film. At these TiO_2 loadings, SWCNT is capable of dispersing TiO_2 particles quite effectively and facilitating charge collection and transportation toward the collecting electrode surface. At higher loadings, a decrease in the photocurrent is observed as it approaches the value obtained in the absence of SWCNT. At these high TiO_2 loadings, the particles may tend to aggregate and most of these TiO_2 aggregates do not make a direct contact with the SWCNT bundles. The photoelectrochemical behavior at high TiO_2 loadings (4 mg/cm^2) thus tends to be similar for both CFE/TiO_2 and CFE/SWCNT/TiO_2. Thus, in an embodiment, beneficial TiO_2 loadings (or other such particles) may be approximately 0.5 to 4 mg/cm^2.

[0047] In order to probe the charge transfer interactions between the excited TiO_2 particles and SWCNT, the current-voltage (I-V) characteristics of the OTE/TiO_2 and OTE/SWCNT/TiO_2 electrodes were analyzed. The films deposited on OTE provided responses similar to those obtained with CFE. In an embodiment, casting of films on OTE allowed annealing of the TiO_2 films at higher temperature (673 K) and better electrochemical performance compared to CFE based electrodes. The I-V characteristics of OTE/TiO_2 and OTE/SWCNT/TiO_2 films in 1 M KOH solution recorded using dark and UV-illumination are shown in FIG. **5**.

[0048] In accordance with an embodiment, the application of anodic bias facilitates charge separation in TiO_2 particulate films. The anodic bias provides the necessary driving force for transport of electrons to the collecting electrode surface and thus minimizes charge recombination. Both OTE/TiO_2 and OTE/SWCNT/TiO_2 exhibit similar enhanced photocurrent response at positive applied potentials. The OTE/SWCNT/TiO_2 exhibits higher photocurrent than OTE/TiO_2, thus confirming the role of a conducting SWCNT scaffold in improving the overall photoelectrochemical performance. However, the potentials corresponding to zero current (often referred to as flat band potential) are different. The flat band potential as recorded from the zero current potential (FIG. **5**) were −0.86 V and −0.79 V versus SCE for TiO_2 and SWCNT/TiO_2 films, respectively. Such a positive shift in the flat band potential is an indication of the electron transfer from TiO_2 to SWCNT as the two systems undergo charge equilibration. Since the conduction band of SWCNT (~0 V versus NHE (normal hydrogen electrode)) is expected to be lower than that of TiO_2 (−0.5 V versus NHE), charge equilibration is expected between the two systems causing the shift of apparent Fermi level to more positive potentials. In an embodiment, a shift of ~70 mV in apparent Fermi level of the SWCNT/TiO_2 system is a further indication that the interplay between the two systems in charge equilibration is an important factor in controlling its photoelectrochemical properties.

[0049] In an embodiment, since the photogenerated holes reaching the electrode surface participate in the water oxidation reaction, one may evaluate the photoconversion efficiency (q) for the water splitting reaction based on the following expression,

$$\eta = \text{power output/incident power} = V_{oc} \times I_{sc} / I_{inc}$$

where V_{oc} refers to open circuit voltage, I_{sc} refers to short circuit current and I_{inc} is the incident light intensity (50 mW/cm^2). If one assumes the electrolysis efficiency proceeds with 100% water splitting reaction, one may use V_{oc} as 1.23 V (the ideal chemical energy limit at 297 K). Using the current value of 36 and 81 μA/cm^2 (obtained independently under no bias conditions), an efficiency of 0.09 and 0.20% may be obtained for OTE/TiO_2 and OTE/SWCNT/TiO_2 electrodes (0.06 and 0.12% for CFE/TiO_2 and CFE/SWCNT/TiO_2).

[0050] In an embodiment, the influence of SWCNT architectures for facilitating charge transport in mesoscopic semiconductor films has been further probed using a TiO_2/Ru(II) trisbipyridyl complex system. Both transient absorption and emission measurements indicate that the SWCNT network in the film has no noticeable influence on the charge injection process from the excited Ru(II) trisbipyridyl complex into TiO_2 particles. However, it plays an important role in improving the charge separation, as the rate of back electron transfer between the oxidized sensitizer (Ru(III)) and the injected electrons becomes slower in the presence of the SWCNT scaffold. The beneficial aspect of charge collection by SWCNT has been further explored by carrying out photoelectrochemical measurements. In an embodiment, dye-sensitized solar cells constructed using this SWCNT scaffold show an improvement in photocurrent generation. However, this improvement in photocurrent generation may be partially neutralized by a lower photovoltage, as the apparent Fermi level of the TiO_2 and SWCNT composite becomes more positive than that of pristine TiO_2.

[0051] In embodiments, semiconductor nanotube assemblies, when assembled on an electrode surface and then modified with dye molecules, offer the possibility to improve the charge collection and transport of charge carriers. While ruthenium is discussed as an exemplary sensitizer, in embodiments, any suitable sensitizer may be utilized, whether a dye, a short bandgap semiconductor, etc. In an embodiment, short bandgap semiconductors such as CdS, PbS, Bi_2S_3, CdSe and

InP may serve as sensitizers as they may transfer electrons to large bandgap semiconductors such as TiO_2 or SnO_2 under visible light excitation.

[0052] In an exemplary embodiment, both OTE/TiO_2 and OTE/SWCNT/TiO_2 films were immersed in an ethanol solution of Ru(II)$(bpy)_2$(dcbpy) (henceforth referred to as Ru(II)) for several hours to facilitate the binding of the dye to the TiO_2 surface.

[0053] In accordance with an embodiment, films of TiO_2 particles may respond solely to UV light as they undergo charge separation upon bandgap excitation (E_g>3.2 eV). When modified with a sensitizer such as Ru(II)$(bpy)_2$ (dcbpy), the TiO_2 particles may directly interact with the excited state of the sensitizer via a charge transfer mechanism (Reactions 1-4):

$$Ru(II)+h\nu \rightarrow Ru(II)^* \quad (1)$$

$$Ru(II)^* \rightarrow Ru(II)+h\nu' \quad (2)$$

$$Ru(II)^*+TiO_2 \rightarrow Ru(II)+TiO_2(e^-) \quad (3)$$

$$Ru(II)+TiO_2(e^-) \rightarrow Ru(II)+TiO_2 \quad (4)$$

[0054] Although a SWCNT does not influence the primary charge injection process in the TiO_2/Ru(II)* system, in an embodiment, it may participate in facilitating charge separation and in promoting electron transport to the electrode surface.

[0055] The results suggest that the photoinjected electrons in TiO_2 survive roughly 50% longer when embedded within the SWCNT network. The equilibration of electrons between SWCNT and TiO_2 results in the transfer of a fraction of electrons into SWCNT, thus stabilizing the photogenerated electrons and reducing the rate of exciton recombination.

[0056] In order to probe the beneficial aspects of a SWCNT network in dye-sensitized solar cells, in accordance with an embodiment, photoelectrochemical cells were constructed using the Ru(II)-modified TiO_2 particulate films as photoanodes. The magnitude of the photocurrent response represents the charge collection efficiency at the electrode surface. FIG. **6**A shows the short-circuit photocurrent generation of the OTE/TiO_2/Ru(II) and OTE/SWCNT/TiO_2/Ru(II) electrodes. Both electrodes were prompt in generating photocurrent with a reproducible response to ON-OFF cycles. It is interesting to note that the films containing a SWCNT network exhibited a roughly 30% higher photocurrent. This increase is greater than the small (2.3%) difference in absorbance between OTE/TiO_2/Ru(II) and OTE/SWCNT/TiO_2/Ru(II) films. On the other hand, the photovoltage (FIG. **6**B) recorded during ON-OFF cycles shows a decreased open-circuit voltage when SWCNT was present in the film.

[0057] The two opposing trends seen in the short-circuit current and open-circuit voltage (FIGS. **6**A and **6**B) may be explained on the basis of the electron capture properties of SWCNT. As the photoinjected electrons are transferred to TiO_2 from excited Ru(II)*, they undergo charge equilibration with SWCNT. This charge equilibration is associated with the shifting of the apparent Fermi level to more positive potentials. A positive shift of tens to hundreds of millivolts in the apparent Fermi level has been noted from the redox equilibration experiments. This shift causes the open-circuit voltage of the photoelectrochemical cell, which is dependent on the difference in Fermi levels between the photoanode and the redox couple, to be lower than that obtained in the absence of SWCNT. The electrons transferred into the SWCNT network may be quickly transported to the collecting electrode surface, minimizing the possibility of charge recombination at grain boundaries. The incorporation of a SWCNT network in the TiO_2 film thus helps to transport electrons through its conductive scaffold and to generate higher photocurrent, at the expense of the open-circuit potential (see FIG. **7**).

[0058] In an embodiment, the electrode performance was further evaluated by recording the IPCE at different incident wavelengths of light. The photocurrent action spectra of the two electrodes under unbiased conditions are shown in FIG. **8**. Both of these electrodes exhibit an IPCE maximum corresponding to the absorption maximum of the Ru(II) complex. In an embodiment, the IPCE response at all wavelengths is enhanced by a factor of ~1.4 as a result of introducing a SWCNT scaffold in the TiO_2 film. Suppressing the back electron transfer and improving the electron transport within the nanostructured TiO_2 film are regarded as the two most important factors controlling the overall IPCE of the cell. Enhancement in the photoconversion efficiency in the present embodiments suggests that charge collection and transport in these films are improved by the SWCNT network.

[0059] In an embodiment, the power characteristics were also evaluated by varying the load resistance (FIG. **9**). A 45% increase in short circuit current seen with the SWCNT nanostructure is consistent with the IPCE and photocurrent measurements described earlier. However, the open-circuit voltage is decreased by about 60 mV as a result of charge equilibration between TiO_2 and SWCNT. A shift in open-circuit potential was also noted in UV-irradiated SWCNT/TiO_2 films. In an embodiment, since the conduction band of SWCNT (~0 V vs. NHE) is expected to be more positive than that of TiO_2 (−0.5 V vs. NHE), charge equilibration is expected between the two systems causing the shift of apparent Fermi level to more positive potentials. Spectroscopic and photoelectrochemical measurements have also confirmed the ability of SWCNT to accept electrons and undergo charge equilibration. The power conversion efficiency for the DSSC's employing OTE/TiO_2/Ru(II) and OTE/SWCNT/TiO_2/Ru(II) electrodes were 0.18% and 0.13%, respectively. The similarity between these two values suggests that improvement in photocurrent may be at least partially nullified by the decrease in photovoltage. As a result of these opposing factors, a small decrease in the fill factor and net power conversion efficiency may be seen.

[0060] In an embodiment, quantum dots, such as CdSe quantum dots, may be assembled on TiO_2 films composed of nanoparticle and/or nanotube morphologies to enhance their function. In an embodiment, the quantum dots may be coupled to the nanoparticles/nanotubes using a bifunctional linker molecule (see FIGS. **10**A and **10**B). The hollow nature of the nanotubes makes both inner and outer surface areas accessible for modification with sensitizing dyes and/or semiconductor quantum dots. Further information regarding quantum dot solar cells and tuning of the photoresponse through size and shape control of the quantum dots may be found in Kongkanand, et al., Quantum Dot Solar Cells—Tuning Photoresponse Through Size and Shape Control of CdSe—TiO_2 Architecture, J. Am. Chem. Soc., Published on Web, Mar. 1, 2008, the entire contents of which are hereby incorporated by reference.

[0061] In accordance with an embodiment, upon bandgap excitation, CdSe quantum dots may inject electrons into TiO_2 nanoparticles/nanotubes, thus enabling the generation of photocurrent in an associated photoelectrochemical solar cell. Embodiments of the invention thus provide: (i) an ability to tune the photoelectrochemical response and/or photoconversion efficiency via size control of quantum dots, and (ii) improvement in photoconversion efficiency by facilitating charge transport through the nanotube architecture.

[0062] In accordance with an embodiment, the IPCE obtained with 3 nm diameter CdSe nanoparticles was 35% for particulate TiO_2 and 45% for tubular TiO_2 morphology. The IPCE observed at the excitonic band increases with decreasing particle size, as the shift in conduction band to more negative potentials increases the driving force and favors fast electron injection. The power conversion efficiency ≦1% obtained with CdSe—TiO_2 nanotube films highlights the usefulness of tubular morphology in facilitating charge transport in nanostructure based solar cells.

[0063] While CdSe quantum dots are discussed throughout this application as exemplary quantum dots, other quantum dots may be utilized, such as PbSe, InAs, etc.

[0064] In an embodiment, various linker molecules may be used to link the quantum dots to the nanoparticles and/or nanotubes. In an embodiment, bifunctional linker molecules, such as MPA (HOOC—CH_2—CH_2—SH), which have both carboxylate and thiol functional groups, facilitate binding between CdSe quantum dots and TiO_2 surfaces. The CdSe quantum dots bound to the TiO_2 surface inherit native quantization properties. The shift in onset absorption with decreasing particle size is similar in both OTE/TiO_2(NP)/CdSe and Ti/TiO_2(NT)/CdSe electrodes. Relatively high absorption of the visible light (absorbance ~0.7) by these electrodes ensures absorbance of more than 80% of the incident light at wavelengths below the onset.

[0065] In accordance with an embodiment, success in achieving relatively high coverage of CdSe quantum dots on these TiO_2 films highlights the ability of small size CdSe quantum dots to penetrate the porous network of a TiO_2 film and provide a uniform coverage throughout the film.

[0066] The open-circuit potential is independent of CdSe particle size indicating that electrons injected from excited CdSe into TiO_2 quickly relax to the lowest conduction band energy. Hence the conduction band level of TiO_2 and the redox potential of the sulfide electrolyte alone dictate an open-circuit voltage of ~600 mV.

[0067] The photocurrent response, however, varies with particle size (see FIGS. **11**A and **11**B). Of those tested, the maximum photocurrent is seen with 3.0 nm diameter CdSe particles. Two opposing effects account for the difference in photocurrent generation at OTE/TiO_2/CdSe electrodes. Decreasing particle size of CdSe increases photocurrent as the shift in conduction band to more negative potentials increases the driving force for charge injection. On the other hand, decreasing the CdSe particle size lowers photocurrent due to an inherently smaller response in the visible region.

[0068] In an embodiment, the photoelectrochemical response may be tuned through size quantization. The photoelectrochemical response of both OTE/TiO_2/CdSe films to monochromatic light irradiation was analyzed in terms of IPCE. The IPCE was determined from short circuit photocurrents (J_{sc}) monitored at different excitation wavelengths (λ) using the expression:

$$IPCE\ \% = \frac{1240 \times J_{short\ circuit}(A/cm^2)}{\lambda\ (nm) \times I_{incident}(W/cm^2)} \times 100\%$$

where $I_{incident}$ is the energy of the monochromatic light incident on the electrode. The IPCE action spectra for OTE/TiO_2(NP)/CdSe and Ti/TiO_2(NT)/CdSe electrodes are presented in FIGS. **12**A and **12**B. The photocurrent action spectra obtained with 3.7, 3.0, 2.6, and 2.3 nm CdSe particles show similar trends for both films. The current peaks may be observed at 580, 540, 520 and 505 nm. Thus, in an embodiment, the photocurrent generation at OTE/TiO_2(NP)/CdSe and Ti/TiO_2(NT)/CdSe electrodes originates from the individual CdSe quantum dots and their size quantization property is responsible for tuning the performance of quantum dot solar cells. In particular, the ability to tune the photoresponse by varying the size of CdSe particles affords the ability to tune the performance of quantum dot solar cells.

[0069] Comparison of IPCE at the excitonic peaks shows an interesting dependence on the particle size. The IPCE values measured at 580 nm (d=3.7 nm), 540 nm (d=3.0 nm), 520 nm (d=2.6 nm) and 505 nm (d=2.3 nm) were 14, 24, 26 and 28% for OTE/TiO_2(NP)/CdSe and 19, 32, 35 and 36% for Ti/TiO_2(NT)/CdSe respectively. It should be noted that the absorbance at the excitonic band was matched to 0.7±0.05. The difference in absorption (≦5%) is smaller than the variation in the IPCE for these four electrodes. Hence, the strong dependence of IPCE on particle size is not due to the relatively small difference in absorption between the two electrodes. The improved IPCE with smaller size quantum dots may arise from the improved rate of electron transfer. The smaller size particles, being more energetic in their excited state, are capable of injecting electrons into TiO_2 at a faster rate.

[0070] It is also interesting to note that the maximum IPCE obtained with CdSe quantum dots linked to TiO_2 particles and tubes are different. The maximum IPCE values in the visible region range from 25% to 35% for OTE/TiO_2(NP)/CdSe electrodes while they vary from 35% to 45% for OTE/Ti/TiO_2(NT)/CdSe electrodes. These IPCE values are relatively higher than those reported in the literature for the sensitization of TiO_2 films (IPCE 25%) and ZnO nanorods (IPCE=18%) with CdSe quantum dots. Note that the comparison made here is based on IPCE or external quantum efficiency values and not based on absorbed light harvesting efficiencies or APCE values.

[0071] Although in embodiments, nanotube TiO_2 films generally absorb more light than nanoparticle TiO_2 films, this difference accounts for a no more than 5% increase in overall photons absorbed. Comparing this with a ~10% improvement in IPCE of the nanotube film over the nanoparticle film, as represented in an exemplary embodiment, demonstrates an advantage of a nanotube architecture for facilitating electron transport in nanostructure based semiconductor films. The electrons in the particulate TiO_2 films are more susceptible to loss at grain boundaries than those in nanotube TiO_2 films. In addition, one also needs to take into consideration the role of crystal structure and surface defects between TiO_2 tubes and particles during their interaction with CdSe quantum dots.

[0072] The open-circuit voltage recorded after stopping the illumination shows slower decrease for Ti/TiO_2(NT)/CdSe than for Ti/TiO_2(NP)/CdSe electrodes. Under open-circuit conditions, electrons may accumulate within the nanostructure semiconductor films following visible irradiation and shift the apparent Fermi level to negative potentials. Once the illumination is stopped, the accumulated electrons may be

slowly discharged as they are scavenged by the redox species in the electrolyte. The slower decay observed with tubular morphology is a further indication that the electrons injected from excited CdSe may survive longer and hence may facilitate electron transport without undergoing losses at the grain boundaries. The results discussed here demonstrate an advantage of assembling semiconductor particles or light harvesting assemblies on nanotube architecture for improving the photocurrent generation efficiency of solar cells.

[0073] In an embodiment, short bandgap semiconductors (e.g., CdS, PbS, Bi_2S_3, CdSe, InP) may be used as sensitizers to extend the photoresponse of TiO_2 into the visible region. CdSe quantum dots are capable of injecting electrons into the conduction band of TiO_2 in a manner analogous to sensitizing dyes. The lower lying conduction band of TiO_2 (−0.5 V vs. NHE) compared to quantized CdSe (≦−1.0 V vs. NHE) is expected to minimize the charge recombination and rectify the transport of charge carriers.

[0074] The CdSe particles exhibit a band edge emission peak which also shifts to the blue region with decreasing particle size. FIG. **13** (a,c) shows the emission spectra of 2.6 and 3.7 nm CdSe quantum dots deposited on glass slides. These quantum dots exhibit characteristic emission peaks at 550 nm and 600 nm respectively. When CdSe is anchored onto a TiO_2 film (b,d) a significant quenching of the emission is seen, thus confirming the excited state interaction between the two semiconductor particles. This quenching behavior represents the deactivation of the excited CdSe via electron transfer to TiO_2 particles. The processes that follow the bandgap excitation of CdSe are presented in Equations 1-3:

$$CdSe+h\nu \rightarrow CdSe(e+h) \rightarrow CdSe+h\nu \quad (1)$$

$$CdSe(e)+TiO_2 \rightarrow CdSe+TiO_2(e) \quad (2)$$

$$CdSe(h)+Red \rightarrow CdSe+Ox \quad (3)$$

[0075] While the electrons injected into TiO_2 are collected to generate photocurrent, in an embodiment, a redox couple may be employed to scavenge the holes (Equation 3). Failure to scavenge holes may lead to surface oxidation, especially during extended periods of irradiation. In a typical photoelectrochemical cell, such oxidation may be minimized by using a sulfide electrolyte.

[0076] The excited CdSe deactivation may be further analyzed by monitoring the emission decay. FIGS. **14**A and **14**B show the emission decay recorded with 2.6 and 3.7 nm CdSe quantum dots. The emission decay was multiexponential as the distribution in the recombination rate constants influenced the decay kinetics. Triexponential decay kinetics were found to be satisfactory in the determination of emission lifetimes. These values were then used to estimate the average lifetime of CdSe emission decay using the following expression:

$$\langle \tau \rangle = \frac{a_1\tau_1^2 + a_2\tau_2^2 + a_3\tau_3^2}{a_1\tau_1 + a_2\tau_2 + a_3\tau_3}$$

[0077] When deposited on a glass slide, 2.6 and 3.7 nm CdSe particles exhibited emission decay with average lifetimes of 4.1 and 7.9 ns respectively. When anchored on TiO_2 particles the average time decreased to 0.4 and 1.3 ns for 2.6 and 3.7 nm diameter CdSe quantum dots respectively. Similar decrease in the CdSe emission lifetime was also seen in the case of TiO_2 nanotubes.

[0078] If one assumes the observed decrease in lifetime to the charge transfer to TiO_2 one can estimate the charge transfer rate constant by the following expression:

$$k_{et} = \frac{1}{\tau_{(CdSe+TiO_2)}} - \frac{1}{\tau_{(CdSe)}}$$

Using observed lifetime values, electron transfer rate constant of 2.5×10^9 s^{-1} and 0.63×10^9 s^{-1} for 2.6 and 3.7 nm diameter CdSe quantum dots on particulate TiO_2 films may be obtained. Similar rate constants were also observed for TiO_2 nanotubes. Similarity between the rate constant values observed for TiO_2 particles and TiO_2 nanotubes indicates that the charge injection dynamics are dictated mostly by the energetics of quantized CdSe particles and not the morphology of the acceptor TiO_2. The conduction band of TiO_2 is at −0.5 V versus NHE. Larger CdSe particles with the bulk properties have band energy close to the reported value of −0.8 V vs. NHE. The difference between the two conduction band energy levels serves as a driving force for the interparticle electron transfer (see FIG. **15**). Since the shift in the conduction band energy is significantly greater than the shift in valence band energy for quantized particles, the conduction band of CdSe quantum dots may be expected to become more negative (on NHE scale) with decreasing particle size. Thus, an increase of a factor of two in the charge injection rate constant may be seen when 2.6 nm CdSe instead of 3.7 nm quantum dots are used.

[0079] In an embodiment, further optimization of cell configuration and improvements in the light absorption properties of the electrodes may be utilized to further improve the performance of quantum dot photovoltaic cells (such as solar cells). In an embodiment, one such approach is the construction of a rainbow solar cell which employs an ordered assembly of nanoparticle quantum dots, such as CdSe, of different diameter. An example of TiO_2 nanotubes decorated with different sized CdSe nanoparticles is shown in FIG. **16**. As white light enters the cell, smaller size nanoparticles (larger bandgap) absorb the portion of the light with smaller wavelengths (blue region). Light with longer wavelengths (red region) which is transmitted through the initial layer is absorbed by subsequent layers, and so on. By creating an orderly gradient of quantum dots of different size, the effective capture of incident light may be enhanced.

[0080] In an embodiment, smaller size particles exhibit higher photoconversion efficiency but absorb less light than larger size particles. In an embodiment, if the quantized particles are anchored on a nanotube array, incident light may be captured while collecting and transmitting electrons through the nanotube network. It is true that the excess energy of electrons of small size particles may be lost once transferred to a supporting manifold; however, such a rainbow cell configuration allows one to couple the faster electron injection rate of small size particles and greater absorption range of large particles effectively.

[0081] Thus, in an embodiment there is provided a nanostructure comprising a nanomaterial comprised of nanoparticles and/or nanotubes, the nanomaterial coupled at one or more locations to a substrate, and a plurality of quantum dots coupled to the nanomaterial, at least two of the plurality of quantum dots being differently sized. In an embodiment, differently sized quantum dots may be randomly distributed on the nanomaterial, or may be ordered, or a combination of random and ordered arrangements may be used. In an embodiment, ordered quantum dots may be arranged with a short wavelength quantum dot located closer to a light source

(such as the sun) than a longer wavelength quantum dot. In such an embodiment, the arrangement of the quantum dots may be done in accordance with the intended direction of the light source, although may contact the quantum dots from other directions as well. In an embodiment, ordered quantum dots may be arranged to form a size gradient (whether partial or completely uniform) with shorter wavelength quantum dots located a greater distance away from the substrate and longer wavelength quantum dots located closer to the substrate.

[0082] In an embodiment there is provided a photovoltaic cell (such as a solar cell) comprising a collecting electrode substrate, a nanomaterial scaffold comprising nanoparticles and/or nanotubes, the nanomaterial scaffold coupled at one or more locations to the substrate, and a plurality of quantum dots and/or nanoparticles coupled to the nanomaterial scaffold. In an embodiment, the collecting electrode substrate may be coupled to or have one or more integrated conducting elements to move the charge/current to a location for use and/or storage. Other components of a photovoltaic cell as known in the art or later developed, such as anti-reflection coatings, concentrating or focusing lenses or other such systems, etc. may be incorporated with embodiments as provided above.

[0083] Although certain embodiments have been illustrated and described herein, it will be appreciated by those of ordinary skill in the art that a wide variety of alternate and/or equivalent embodiments or implementations calculated to achieve the same purposes may be substituted for the embodiments shown and described without departing from the scope of the present invention. Those with skill in the art will readily appreciate that embodiments in accordance with the present invention may be implemented in a very wide variety of ways. This application is intended to cover any adaptations or variations of the embodiments discussed herein. Therefore, it is manifestly intended that embodiments in accordance with the present invention be limited only by the claims and the equivalents thereof.

What is claimed is:

1. A nanostructured material, comprising:

a single wall carbon nanotube having a first and second end and an outer and inner surface, the first end of the single wall carbon nanotube coupled to a substrate; and

a plurality of nanoparticles coupled to the single wall carbon nanotube.

2. The nanostructured material of claim **1**, wherein the nanoparticles comprise at least one of TiO_2 and SnO_2.

3. The nanostructured material of claim **1**, wherein at least one of the plurality of nanoparticles is coupled to the outer surface of the single wall carbon nanotube.

4. The nanostructured material of claim **1**, wherein at least one of the plurality of nanoparticles is coupled to the inner surface of the single wall carbon nanotube.

5. The nanostructured material of claim **1**, wherein the nanoparticles are loaded on the single wall carbon nanotube at approximately 0.5 to 4 mg/cm^2.

6. The nanostructured material of claim **1**, wherein the substrate is configured to accept electrons traveling through the single wall carbon nanotube to create a current.

7. The nanostructured material of claim **1**, further comprising one or more quantum dots coupled to the single wall carbon nanotube and/or coupled to one or more of the plurality of nanoparticles.

8. The nanostructured material of claim **7**, wherein the one or more quantum dots are coupled to the single wall carbon nanotube and/or coupled to one or more of the plurality of nanoparticles via a linker molecule.

9. The nanostructured material of claim **7**, wherein the one or more quantum dots comprise at least one of CdSe, CdTe, PbSe, and InAs.

10. The nanostructured material of claim **7**, wherein at least one of the one or more quantum dots is coupled to the outer surface of the single wall carbon nanotube.

11. The nanostructured material of claim **7**, wherein at least one of the one or more quantum dots is coupled to the inner surface of the single wall carbon nanotube.

12. The nanostructured material of claim **1**, further comprising one or more sensitizers coupled to the single wall carbon nanotube and/or coupled to one or more of the plurality of nanoparticles.

13. The nanostructured material of claim **12**, wherein the one or more sensitizers comprise a dye.

14. The nanostructured material of claim **13**, wherein the dye is ruthenium.

15. The nanostructured material of claim **12**, wherein the one or more sensitizers comprise a short bandgap semiconductor.

16. The nanostructured material of claim **15**, wherein the short bandgap semiconductor is at least one of CdS, PbS, Bi_2S_3, CdSe and InP.

17. A nanostructure comprising:

a nanomaterial comprised of nanoparticles and/or nanotubes, the nanomaterial coupled at one or more locations to a substrate; and

a plurality of quantum dots coupled to the nanomaterial, at least two of the plurality of quantum dots being differently sized.

18. The nanostructure of claim **17**, wherein the differently sized quantum dots are randomly distributed on the nanomaterial.

19. The nanostructure of claim **17**, wherein the differently sized quantum dots are ordered on the nanomaterial.

20. The nanostructure of claim **19**, wherein the ordered quantum dots are arranged with a short wavelength quantum dot located closer to a light source than a longer wavelength quantum dot.

21. The nanostructure of claim **19**, wherein the ordered quantum dots are arranged to form a size gradient with shorter wavelength quantum dots located a greater distance away from the substrate and longer wavelength quantum dots located closer to the substrate.

22. The nanostructure of claim **17**, wherein the one or more quantum dots are coupled to the nanomaterial via a linker molecule.

23. A photovoltaic cell, comprising:

a collecting electrode substrate;

a nanomaterial scaffold comprising nanoparticles and/or nanotubes, the nanomaterial scaffold coupled at one or more locations to the substrate; and

a plurality of quantum dots and/or nanoparticles coupled to the nanomaterial scaffold.

* * * * *